Published in final edited form as:
J Endod. 2011 June ; 37(6): 745–752. doi:10.1016/j.joen.2011.02.022.

Dental MRI: Making the Invisible Visible

Djaudat Idiyatullin, PhD[1], **Curt Corum, PhD**[1], **Steen Moeller, PhD**[1], **Hari S. Prasad, BS, MDT**[2], **Michael Garwood, PhD**[1], and **Donald R. Nixdorf, DDS, MS**[3]

[1] The Center for Magnetic Resonance Research and Department of Radiology, University of Minnesota, 2021 6th St. SE, Minneapolis, Minnesota 55455 USA

[2] Division of Oral Pathology in the Department of Diagnostic & Biological Sciences, University of Minnesota, 16-110 Moos Tower 515 Delaware St. SE, Minneapolis, Minnesota 55455 USA

[3] Division of TMD & Orofacial Pain in the Department of Diagnostic & Biological Sciences and Department of Neurology, University of Minnesota, 6-320 Moos Tower 515 Delaware St. SE, Minneapolis, Minnesota 55455 USA

Abstract

Introduction—Clinical dentistry is in need of non-invasive and accurate diagnostic methods to better evaluate dental pathosis. The purpose of this work was to assess the feasibility of a recently developed magnetic resonance imaging (MRI) technique, called SWeep Imaging with Fourier Transform (SWIFT), to visualize dental tissues.

Methods—Three *in vitro* teeth, representing a limited range of clinical conditions of interest, imaged using a 9.4T system with scanning times ranging from 100 seconds to 25 minutes. *In vivo* imaging of a subject was performed using a 4T system with a 10-minute scanning time. SWIFT images were compared with traditional two-dimensional radiographs, three-dimensional cone-beam computed tomography (CBCT), gradient-echo MR imaging technique, and histological sections.

Results—A resolution of 100 microns was obtained from *in vitro* teeth. SWIFT also identified the presence and extent of dental caries and fine structures of the teeth, including cracks and accessory canals, which are not visible with existing clinical radiography techniques. Intraoral positioning of the radiofrequency coil produced initial images of multiple adjacent teeth at a resolution of 400 microns.

Conclusions—SWIFT MRI offers simultaneous three-dimensional hard and soft tissue imaging of teeth without the use of ionizing radiation. Further, it has the potential to image minute dental structures within clinically relevant scanning times. This technology has implications for endodontists since it offers a potential method to longitudinally evaluate teeth where pulp and root structures have been regenerated.

The authors report the following potential conflict of interest: Dr. Garwood has an equity interest in SSI, Drs Idiyatullin, Moeller and Nixdorf are consultants for SSI, and Drs Corum, Garwood, Idiyatullin, Moeller, are entitled to sales royalty through the University of Minnesota for products related to the research described in this paper. These relationships have been reviewed and managed by the University of Minnesota in accordance with its conflict of interest policies.

INTRODUCTION

Diagnostic imaging in dentistry depends mostly on X-ray-based techniques that carry some risks and limitations, such as: exposure to ionizing radiation and its associated increased risk of cancer (1) and inability to visualize the pulpal tissue (2). The application of X-ray-based three-dimensional diagnostic imaging is likely to increase in endodontics as cone-beam computed tomography (CBCT) imaging systems become more available (3, 4). However, besides exposure to radiation, such systems cannot simultaneously image calcified and non-calcified dental tissues, which is a significant limitation, particularly as regenerative endodontic procedures become more common in clinical practice (5).

In a recent review of parameters used in diagnostic testing for assessing pulpal and periapical tissues the following conclusion was highlighted: "…diagnosis of dental pulp diseases suffers from the operator's inability to test/or image that tissue directly because of its location within a relatively hard tissue, dentin." (2). This review also outlined technical advances underway to address these limitations, but did not include magnetic resonance imaging techniques. This is justified due to the technical challenges with this diagnostic technique that severely inhibits endodontic application at this time, which is likely the reason behind the paucity of research on the topic.

Magnetic resonance imaging (MRI) has become an indispensable tool for noninvasively diagnosing and monitoring disease in soft tissues, without using ionizing radiation. In biological tissues, the MRI signals measured arise from the spinning magnetic moments of the hydrogen nuclei in water molecules (hereafter called "water signal" or "signal"). The water signal is detectable after a radiofrequency (RF) pulse is applied, which causes the nuclear spins to resonate in the strong static magnetic field. Conventional MRI cannot easily visualize teeth because of their high mineral content; minerals occupy 50% of a tooth's dentin and 90% of its enamel by volume, with water and proteins occupying the rest (6). Also, since the water signal has a highly restricted molecular motion within these densely mineralized tissues, the signal decays very quickly after RF excitation. The time constant describing the signal's free induction decay (FID) is known as the transverse relaxation time (T_2). The FID of mineralized dental tissue has multiple components, with a mean T_2 of about 200 μs (7) for the dentin and 60 μs (8) for the enamel. These time intervals are less than those needed for conventional MRI pulse sequences to accomplish spatial encoding with pulsed magnetic field gradients, which typically requires more than 1 ms. In other words, the signal from mineralized dental tissues decays before MRI signal digitization occurs, resulting in MRI images with little or no image intensity (black zone). Consequently, conventional MRI techniques in dentistry have been restricted to imaging pulp, attached periodontal membrane, and other surrounding soft tissues, or have required indirect imaging of enamel and dentin through contrast produced by MRI-visible medium (9–13).

Images of the mineralized components of dental tissues have been obtained from extracted teeth by using solid-state MRI techniques, such as single point imaging (14) and stray-field imaging (15). However, with imaging times in the 5 to 6 hour range, such methods are unsuitable for *in vivo* applications. Alternatively, FID-projection reconstruction techniques (16, 17) can also be used to image fast relaxing objects. Unfortunately these techniques are severely limited by the achievable RF pulse amplitude, especially with low efficiency RF coils typically used in clinical MRI, which reduces the achievable signal-to-noise ratio (SNR). Dental imaging is challenging even for Ultrashort TE (UTE) (18, 19), the most mature clinical MRI technique for visualizing tissues with very short T_2. The ability of UTE methods to visualize dentin and enamel is limited by the time required to perform RF excitation and to ramp-on the readout gradient (20). To our knowledge, none of the existing

MRI-based techniques have produced diagnostic-quality images of calcified teeth structures within clinical-acceptance scanning times.

Our recently developed MRI method called SWeep Imaging with Fourier Transformation (SWIFT) (21) overcomes many of the difficulties of detecting fast relaxing signals. SWIFT uses a swept RF excitation and simultaneous signal acquisition in a time-shared mode in the presence of field gradients. This allows for the imaging of objects with truly ultra-short T_2 with relatively low peak RF amplitude, and unlike the UTE technique, greatly reduced demand on the scanner's gradient hardware. The purpose of our study was to assess the feasibility of this MRI method to visualize calcified and non-calcified dental tissues, as well as compare SWIFT images with traditional X-ray modalities and histological sections, where appropriate, to highlight its potential for clinical dental application. The initial focus of this research was to demonstrate the ability to visualize calcified dental tissues in addition to pulpal and periradicular tissues which have previously been visualized by MRI (11, 22, 23).

Materials and Methods

Teeth samples

Three extracted teeth were selected for *in vitro* imaging, harvested as waste tissue without maintaining any patient identifying data, making their use exempt under current Institutional Review Board protocols. Following extraction, the teeth were stored in an isotonic saline solution, containing 0.1% of sodium azide as an antimicrobial, for up to 3 days before conducting all MRI experiments. Immediately prior to MRI experiments, the teeth were wiped with a paper towel to remove any free water on the surface.

To test the ability of SWIFT MRI to assess the extent of dental caries, the components of the pulp and overall tooth anatomy, we selected a mandibular right second molar tooth that had both diagnostically obvious interproximal caries and questionable occlusal caries (Tooth 1) (Fig 1,2). To test the ability to assess pulpal reaction to repeated, longstanding dental injury, we selected a maxillary right central incisor with multiple composite resin restorations and recurrent caries (Tooth 2) (Fig 3,4). For the third example, we chose an intact left maxillary first premolar (Tooth 3) in which a complete lingual cusp fracture was induced prior to MR imaging to assess the possibility of visualizing cracks within teeth, something that is not reliably obtained in clinical practice (24) (Fig 5).

In vivo imaging was performed on a healthy volunteer, who was one of the researchers (DRN). To further demonstrate the feasibility of clinical applications, posterior teeth with amalgam restorations were imaged (Figs. 6 and 7). This research application was also reviewed and determined to be exempt by the Institutional Review Board.

Radiographs

Periapical and bitewing radiographs were obtained on a digital sensor (Prof Suni v3.9.0.42, Suni Medical Imaging, San Jose, CA) with the X-ray source coming from the dental tube head (GE1000, Milwaukee, WI). The sensor was 500 mm from the tube head. Exposure time was 0.2 seconds at 12 mA and 100 kVp.

Three-dimensional CBCT (17–19 iCAT, Imaging Sciences, Hatfield, PA) was obtained in one scan, with a 60 mm field of view (FOV) at 37 mA/sec for 27 seconds and 120 kV with a resolution of 0.2 mm.

Histology

Teeth were stored in 10% neutral buffered formalin and sectioned into apical and coronal halves. Tissue was dehydrated with graded concentrations of alcohol over 9 days in a serial fashion. Following dehydration, the specimens were infiltrated with a light-curing embedding resin (Technovit 7200VLC, Kulzer, Wehrheim, Germany) for 20 days with constant shaking at normal atmospheric pressure. The teeth were then polymerized by using 450 nm light at a temperature range of 35°C–40°C. An EXAKT cutting/grinding system (EXAKT Technologies, Oklahoma City, OK) was used to prepare teeth sections of 150 μm thickness. Sections were polished to a thickness of 40–50 μm with a series of polishing sandpaper discs (800 to 2400 grit), followed by a final polish with 0.3 micron alumina polishing paste. Sections were stained with Stevenel's blue and Van Gieson's picro fuchsin, and then mounted on slides and cover-slipped.

MRI experiments

All *in vitro* MRI experiments were performed in a 31-cm, 9.4-T magnet (Magnex Scientific, Abingdon, UK) equipped with a Varian Inova console (Varian Inc., Palo Alto, CA). RF transmission and signal reception were performed with a home built, single loop, 25 mm-diameter coil.

In the SWIFT sequence, RF excitation was performed with a hyperbolic secant pulse (25) having a time-bandwidth product of 256, an excitation bandwidth of 125 kHz, and a flip angle of 15°. The pulse was oversampled by a factor of 32 (26). Data were collected in 256 pulse gaps of 6 μs duration each. The repetition time (TR), including 2 ms pulse length, was 2.5 ms. Data in k-space consisted of 32,000 spokes for medium resolution images and 128,000 spokes for high resolution images. The terminus of the k-space vectors describe the isotropically distributed points on a sphere located in up to 32 interleaved spirals (27). The total acquisition time was equal to 100 seconds for the medium resolution images collected without signal averaging and about 24 minutes for high resolution images using 4 signal averages.

In the gradient-echo (GRE) sequence, experimental parameters were as follows: 30° (flip angle), 13.5 ms (TR), 3 ms (TE), 80 kHz (bandwidth), 256 complex points in each of 65,536 (256×256) phase encode steps and total acquisition time 14 minutes.

In vivo SWIFT experiments were performed in a 90-cm, 4-T magnet (Oxford Magnet Technology, Oxon, UK) interfaced to a Varian DirectDrive console. RF transmission and signal reception were performed with custom fabricated coils of intra-oral configuration. The coil was a one-side shielded single-loop of 40 mm diameter located between the cheek and teeth (Fig 6) and held in relation to the occlusal plane with a 2 mm thick Teflon bite fork. Isolation of the coil from the oral environment was achieved by covering the coil with Teflon wrapping. The SWIFT images (Fig 7) were acquired without averaging using 8° (flip angle), 62 kHz (bandwidth) and 128,000 spokes consisting of 16 interleaved groups, with total acquisition time 10 minutes. The rest of parameters were same as for *ex vitro* experiments. The "rigid body" motions were detected by comparing 16 low resolved images reconstructed for each interleaved group individually. The manually estimated correction angles and translation coefficients were subsequently used during reconstruction of the presented high-resolution images.

RESULTS

Tooth anatomy and dental caries in SWIFT images

In the SWIFT images, the dental anatomy is well resolved, including enamel, dentin and pulpal structures (Fig 1). As expected, enamel with its lower water content and shorter T_2 exhibits less intense signal than dentin. The relative intensities from regions-of-interest placed in pulp tissue, dentin, and enamel are approximately 100:35:10. For comparison, the relative water composition by volume in these tissues is known to be 100:20:8 (6). Although a more accurate comparison must also account for differences in the relaxation parameters of these tissues, it can be concluded that these SWIFT images do not have appreciable T_2 weighting (unlike GRE images as shown below in Fig 3) and all dental tissues are visible.

The interproximal caries on the distal aspect of the crown (left side of tooth) are readily visualized with all imaging modalities. However, the hyper-intense region in the SWIFT images (Figure 2, S1b, S1c) clearly delineates the extent of demineralization towards the pulp, as verified in the histological sections. Neither radiographic imaging modality could measure the extent of demineralization as well as SWIFT. Moreover, the radiograph modalities do not reveal the early extension of the occlusal caries into the dentin (Figure 2, S1b). This extension is only suggested by the presence of staining within the pits and fissures of the tooth, but is well demarcated by SWIFT.

The bright signal on the surface of the tooth roots originates from cementum and attached residual periodontal ligament, which is retained following routine teeth extractions.

Composite restorations and calcified coronal pulp in SWIFT images

In the images produced by X-ray methods, the composite resin restorations appear radiopaque (bright) or radiolucent (dark) (Fig 3), because the resins have different concentrations of heavy metal or minerals that block radiation to assist with diagnosing recurrent caries (28). The recurrent caries located on the gingival margins of the restorations are visible as radiolucent areas and can be difficult to diagnose when adjacent to radiolucent composite restorations. Fortunately, both types of composite resin materials have short T_2 and exhibit low intensity in SWIFT images, and are therefore unlikely to be misdiagnosed as caries. The dentin of the whole tooth is well visualized, including the reparative dentin that has replaced the coronal pulp, presumably due to the history of past disease, multiple existing restorations, and present recurrent caries. This replacement of the coronal pulp by mineralized tissue is suggested by the periapical radiograph and clearly demonstrated by the CBCT (Fig 3). In the GRE image (Fig 3) however all hard tissues including dentin are invisible which makes diagnosis more difficult.

SWIFT can visualize anatomical details that are not observable by existing clinical imaging techniques. In this same sample tooth, an accessory canal within the apical one-third of the root apex (confirmed by histological sectioning, see Figure 4) can be identified by SWIFT, but not by the other imaging modalities. Likely, the interface between water and dentin within this accessory canal creates a susceptibility-induced blurring that magnifies the presence of this anatomical structure. Additionally, as in Figure 1, the tooth's cementum and periodontal ligament that surrounds the apical half of the tooth are easily identified given their sufficiently high water content.

Tooth fractures in SWIFT images

The induced lingual cusp complete fracture (Fig 5, yellow arrows), which was closely reapproximated as seen in the optical images, was easy to identify in SWIFT images as compared to images produced by radiographic modalities. The periapical radiograph, taken

in the mesiodistal orientation, provides the best radiographic evidence of the crack, but such an imaging orientation cannot be obtained clinically since the alveolar bone would be located where the X-ray sensor was placed. In one of the SWIFT images, trapped air is visible as a black zone within the pulp (Fig 3, red arrow); this likely occurred following fracturing.

Preliminary *in vivo* SWIFT images of teeth

In vivo SWIFT imaging of teeth is technically more challenging than *in vitro* imaging due to three main factors: 1) subject motion, 2) proximity of intense signal from surrounding soft tissue, and 3) enlarged FOV. In the absence of compensating measures, these factors can diminish image quality.

To overcome these challenges and to achieve dental imaging in a practical scanning time with SWIFT, a one-side shielded intra-oral coil was designed and constructed. RF shielding on the backside of the coil greatly minimized signal from the cheek (Fig 6). Additionally, during image reconstruction we applied a simple motion correction to compensate “rigid motion” of head (see Methods).

In Figure 7, *in vivo* SWIFT images are presented from our first attempt to solve the technical problems highlighted above and demonstrate the feasibility of *in vivo* dental MRI. The grey scale used to display the SWIFT images was adjusted to highlight calcified features of the teeth. As a result of this scaling, the cancellous bone, mucosa and gingival tissues appear bright and cannot be discerned from each other. The subject has metallic restorations (amalgam) within both maxillary molars and the mandibular first molar, which is visible in the photographs and bitewing radiograph. Such restorations commonly create a streaking artifact in CBCT images that greatly reduces the diagnostic utility of this three-dimensional radiographic technique for imaging teeth and associated structures (29). Due to the shortness of the delay between excitation and acquisition in SWIFT, the method is relatively insensitive to magnetic susceptibility artifacts created by such metallic restorations.

DISCUSSION

Our results demonstrate that MRI with SWIFT can simultaneously image both hard and soft dental tissues with high resolution in short enough scanning times to be practical for clinical applications. With SWIFT, minute details not observed with currently available clinical imaging techniques can be visualized within three-dimensions without the use of ionizing radiation. Case reports and series support the notion that there is value gained with three-dimensional diagnostic imaging techniques when applied to the field of endodontics (3, 30). Also, at present there does not seem to be an acceptable method for *in vivo* evaluation of the contribution accessory canals, filled or unfilled, have on the outcome of endodontic treatment (31), which is a clinical issue that may also be able to be addressed with the development of dental MRI. Furthermore, SWIFT-based MRI has the potential to precisely determine the extent of carious lesions and simultaneously assess pulpal tissue (not shown here), which would be an important step towards being able to distinguish between reversible and irreversible pulpitis (32).

With simultaneous RF excitation and signal acquisition, SWIFT obtains signal from densely calcified tissues that have fast decaying signal, produces less distortion in the presence of materials that have magnetic susceptibility, and is less sensitive to motion artifacts– overcoming three significant barriers inhibiting MRI use for dental applications. Also, the SWIFT method is nearly 50 dB quieter than a comparable MRI exam that uses traditional, GRE, MRI pulse sequences (33).

The main weakness of MRI methods in comparison with traditional dental imaging is the high cost, differential and limited accessibility of MRI equipment. It is anticipated that the development of this imaging technique will likely follow a similar course as CT-based imaging: from proof-of-concept application to technology refinement that allows first application for research purposes, followed by use for restricted application to address unmet needs in specialty fields and ultimately to the development of point-of-care diagnostics. Furthermore, the cost of SWIFT-based MRI systems might be reduced, when compared with traditional MRI, due to the method's reduced slew rate requirement on the gradient amplifiers and its increased tolerance to magnet inhomogeneity.

In vivo imaging was performed with a 4T research scanner that provided the needed experimental capabilities and flexibility to execute the SWIFT sequence. The lower field strengths of clinical MRI scanners (typically 1.5 or 3 Tesla) can also be used, but with an approximately linear decrease in SNR (34). However, based on our preliminary experience, it can be concluded that the quality of *in vivo* images and the achievable resolution are not limited by SNR, but depend highly on coil configuration, patient comfort, and motion control, all of which are not dependent on field strength and also believed to be successfully addressed with future research at these lower field strengths. At present, however, the spatial resolution (~0.4 mm) of the obtained *in vivo* SWIFT images is probably two-fold coarser than what will be needed for clinical use. However, by further optimizing the coil configuration (35) and applying a parallel imaging strategy, improvements in resolution should be achievable in the future. Additional effort should be made to minimize motion artifacts, which is an ongoing concern for all diagnostic imaging systems. Addressing these technical issues would produce an imaging system that could simultaneously evaluate the growth and development of calcified and pulpal tooth structures, as well as the periradicular tissues, in three-dimensions without the use ionizing radiation. This MRI technology might also enable longitudinal clinical studies of patients who received regenerative endodontic treatments.

In conclusion, magnetic resonance imaging based on the SWIFT technique offers simultaneous three-dimensional hard and soft tissue imaging of teeth in clinically relevant scanning times without subjecting patients to ionizing radiation. The development of this technology has many potential applications in dentistry and may radically change diagnostic imaging.

Acknowledgments

This work was supported by the NIH Grants P41-RR008079, K12-RR023247, S10-RR023730 and by the Keck Foundation. The authors thank the Division of Oral and Maxillofacial Surgery at the University of Minnesota School of Dentistry for providing tissue samples, Dr. Vladimir Leon-Salazar for taking the optical images, and Drs. Dorothy Semenov & Anne Marie Weber-Main for critically reviewing and editing manuscript drafts.

References

1. Longstreth WT Jr, Phillips LE, Drangsholt M, Koepsell TD, Custer BS, Gehrels JA, et al. Dental X-rays and the risk of intracranial meningioma: a population-based case-control study. Cancer. 2004; 100:1026–34. [PubMed: 14983499]
2. Newton CW, Hoen MM, Goodis HE, Johnson BR, McClanahan SB. Identify and Determine the Metrics, Hierarchy, and Predictive Value of All the Parameters and/or Methods Used During Endodontic Diagnosis. J Endod. 2009; 35:1635–44. [PubMed: 19932338]
3. Kottoor J, Velmurugan N, Sudha R, Hemamalathi S. Maxillary first molar with seven root canals diagnosed with cone-beam computed tomography scanning: a case report. J Endod. 2010; 36:915–21. [PubMed: 20416446]

4. Blattner TC, George N, Lee CC, Kumar V, Yelton CD. Efficacy of cone-beam computed tomography as a modality to accurately identify the presence of second mesiobuccal canals in maxillary first and second molars: a pilot study. J Endod. 2010; 36:867–70. [PubMed: 20416435]
5. Hargreaves, K.; Law, A. Cohen's Pathways of the Pulp. 10. St. Louis, MO: Mosby Elsevier; 2010. Regenerative endodontics; p. 602-19.
6. Pasteris JD, Wopenka B, Valsami-Jones E. Bone and Tooth Mineralization: Why Apatite? ELEMENTS. 2008; 4:97–104.
7. Schreiner LJ, Cameron IG, Funduk N, Miljkovic L, Pintar MM, Kydon DN. Proton NMR spin grouping and exchange in dentin. Biophys J. 1991; 59:629–39. [PubMed: 2049523]
8. Funduk N, Kydon DW, Schreiner LJ, Peemoeller H, Miljkovic L, Pintar MM. Composition and relaxation of the proton magnetization of human enamel and its contribution to the tooth NMR image. Magn Reson Med. 1984; 1:66–75. [PubMed: 6571438]
9. Olt S, Jakob PM. Contrast-enhanced dental MRI for visualization of the teeth and jaw. Magn Reson Med. 2004; 52:174–6. [PubMed: 15236382]
10. Tutton LM, Goddard PR. MRI of the teeth. Br J Radiol. 2002; 75:552–62. [PubMed: 12124246]
11. Lockhart PB, Kim S, Lund NL. Magnetic resonance imaging of human teeth. J Endod. 1992; 18:237–44. [PubMed: 1402579]
12. Weglarz WP, Tanasiewicz M, Kupka T, Skorka T, Sulek Z, Jasinski A. 3D MR imaging of dental cavities--an in vitro study. Solid State Nucl Magn Reson. 2004; 25:84–7. [PubMed: 14698391]
13. Tymofiyeva O, Rottner K, Gareis D, Boldt J, Schmid F, Lopez MA, et al. In vivo MRI-based dental impression using an intraoral RF receiver coil. Conc Magn Reson B: Magn Reson Eng. 2008; 33B:244–51.
14. Appel TR, Baumann MA. Solid-state nuclear magnetic resonance microscopy demonstrating human dental anatomy. Oral Surg Oral Med Oral Pathol Oral Radiol Endod. 2002; 94:256–61. [PubMed: 12221396]
15. Lloyd CH, Scrimgeour SN, Hunter G, Chudek JA, Lane DM, Mcdonald PJ. Solid state spatially resolved ^{1}H and ^{19}F nuclear magnetic resonance spectroscopy of dental materials by stray-field imaging. J Mater Sci Mater Med. 1999; 10:369–73. [PubMed: 15348138]
16. Hafner S. Fast imaging in liquids and solids with the Back-projection Low Angle ShoT (BLAST) technique. Magn Reson Imaging. 1994; 12:1047–51. [PubMed: 7997092]
17. Madio DP, Lowe IJ. Ultra-fast imaging using low flip angles and FIDs. Magn Reson Med. 1995; 34:525–9. [PubMed: 8524019]
18. Bergin CJ, Pauly JM, Macovski A. Lung parenchyma: projection reconstruction MR imaging. Radiology. 1991; 179:777–81. [PubMed: 2027991]
19. Gatehouse PD, Bydder GM. Magnetic resonance imaging of short T_2 components in tissue. Clin Radiol. 2003; 58:1–19. [PubMed: 12565203]
20. Carl, M.; Chiang, J-TA.; Han, E.; Bydder, G.; King, K. Bloch Simulations of UTE, WASPI and SWIFT for Imaging Short T2 Tissues. ISMRM Annual Scientific Meeting & Exhibition; 2010 May 1 – May 7; Stockholm, Sweden. 2010. p. 884
21. Idiyatullin D, Corum C, Park J-Y, Garwood M. Fast and quiet MRI using a swept radiofrequency. J Magn Reson. 2006; 181:342–9. [PubMed: 16782371]
22. Ploder O, Partik B, Rand T, Fock N, Voracek M, Undt G, et al. Reperfusion of autotransplanted teeth--comparison of clinical measurements by means of dental magnetic resonance imaging. Oral Surg Oral Med Oral Pathol Oral Radiol Endod. 2001; 92:335–40. [PubMed: 11552155]
23. Kress B, Buhl Y, Anders L, Stippich C, Palm F, Bahren W, et al. Quantitative analysis of MRI signal intensity as a tool for evaluating tooth pulp vitality. Dentomaxillofac Radiol. 2004; 33:241–4. [PubMed: 15533978]
24. Rivera, E.; Walton, R. Cracking the cracked tooth code: Detecting and treatment of various longitudinal tooth fractures. Chicago, IL: American Association of Endodontists; 2008.
25. Tannus A, Garwood M. Improved Performance of Frequency-Swept Pulses Using Offset-Independent Adiabaticity. J Magn Reson. 1996; A 120:133–7.
26. Idiyatullin D, Corum C, Moeller S, Garwood M. Gapped pulses for frequency-swept MRI. J Magn Reson. 2008; 193:267–73. [PubMed: 18554969]

27. Wong ST, Roos MS. A strategy for sampling on a sphere applied to 3D selective RF pulse design. Magn Reson Med. 1994; 32:778–84. [PubMed: 7869901]

28. Wenzel, A. Dental caries. In: White, SC.; Pharoah, MJ., editors. Oral Radiology: Principles and Interpretation. 6. St. Louis, MO: Mosby Elsevier; 2009. p. 270-81.

29. Barrett JF, Keat N. Artifacts in CT: Recognition and Avoidance. Radiographics. 2004; 24:1679–91. [PubMed: 15537976]

30. Lofthag-Hansen S, Huumonen S, Grondahl K, Grondahl HG. Limited cone-beam CT and intraoral radiography for the diagnosis of periapical pathology. Oral Surg Oral Med Oral Pathol Oral Radiol Endod. 2007; 103:114–9. [PubMed: 17178504]

31. Ricucci D, Siqueira JF Jr. Fate of the tissue in lateral canals and apical ramifications in response to pathologic conditions and treatment procedures. J Endod. 2010; 36:1–15. [PubMed: 20003929]

32. Levin LG, Law AS, Holland GR, Abbott PV, Roda RS. Identify and Define All Diagnostic Terms for Pulpal Health and Disease States. J Endod. 2009; 35:1645–57. [PubMed: 19932339]

33. Corum, C.; Idiyatullin, D.; Moeller, S.; Garwood, M. Progress in 3d Imaging at 4 T with SWIFT. ISMRM 16th Scientific Meeting & Exhibition; 2008 3–9 May; Toronto, Ontario, Canada. 2008.

34. Vlaardingerbroek, MT.; den Boer, JA. Magnetic Resonance Imaging- Theory and Practice. 3. New York: Springer-Verlag; 2003.

35. Roemer PB, Edelstein WA, Hayes CE, Souza SP, Mueller OM. The NMR phased array. Magn Reson Med. 1990; 16:192–225. [PubMed: 2266841]

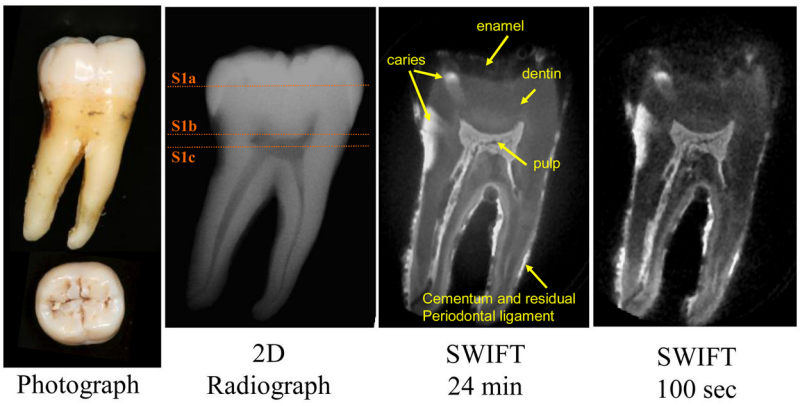

Figure 1.

A mandibular right second molar (Tooth 1) with obvious interproximal and questionable occlusal caries, imaged with different modalities. Two SWIFT images with different scanning times (24 minutes and 100 seconds) are presented. The image acquired in 100 seconds has more noise, but the tooth structure and dental caries are still well recognizable. The application of an additional filtering step is a potential way to increase the SNR ratio and thus produce satisfactory quality images at shorter scanning times. (SWIFT: selected slices with FOV diameter 25 mm and isotropic voxel size 98 μm; CBCT: isotropic voxel size 200 μm)

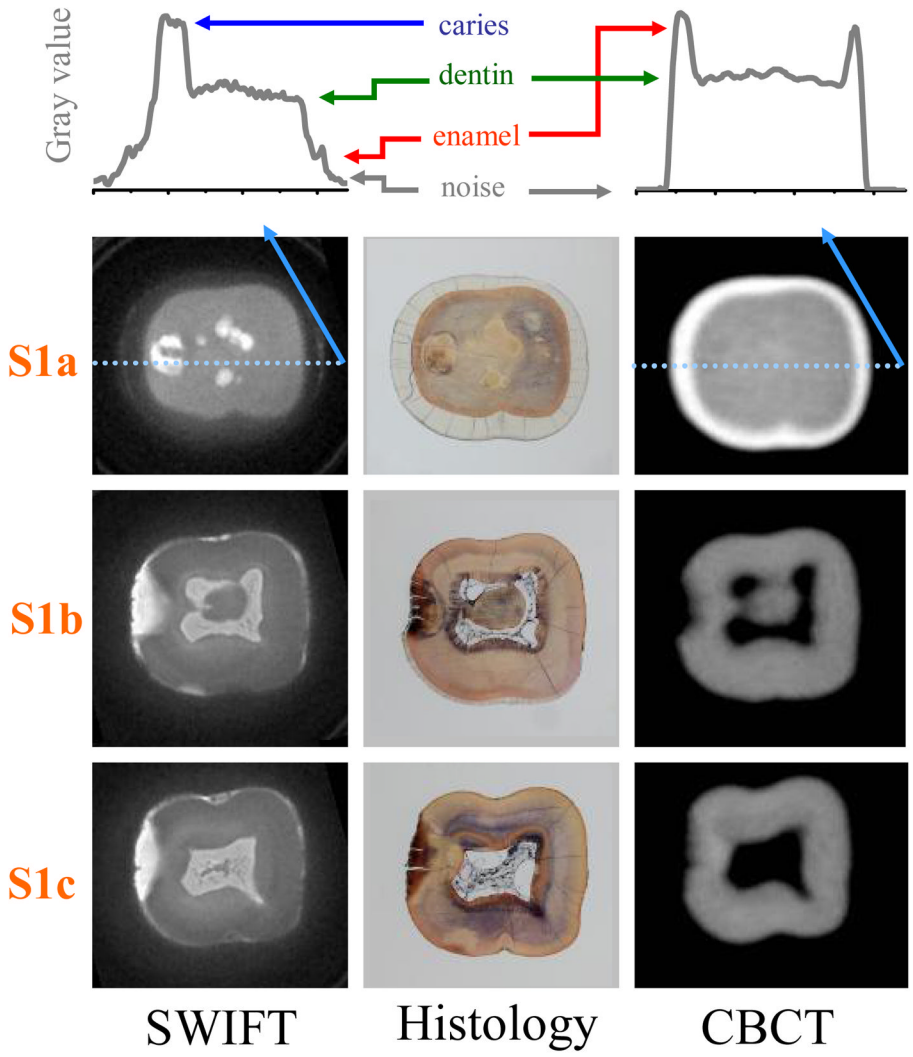

Figure 2.

Three cross-sectional slices of Tooth 1 (marked as S1a, S1b and S1c in Figure 1) are presented. Graphs located on the top of figure with arbitrary gray value present the profiles of slice S1a at the position depicted with a light blue line. The colored arrows delineate the surface of the tooth enamel (red), sound dentin (green) and the signal level of caries (dark blue), respectively. Note that the signal from enamel tissue in SWIFT image is clearly greater than background noise (black arrows). The presence of occlusal caries is observed in S1a within the SWIFT and non-decalcified histology sections, which is the gold-standard measure, but not observed in the CBCT scan. The extent of the interproximal caries towards the dental pulp, in S1b and S1c, are more completely delineated in the SWIFT sections than the CBCT when compared to histology. The slice thickness is equal to 98 μm for SWIFT and 200 μm for CBCT images.

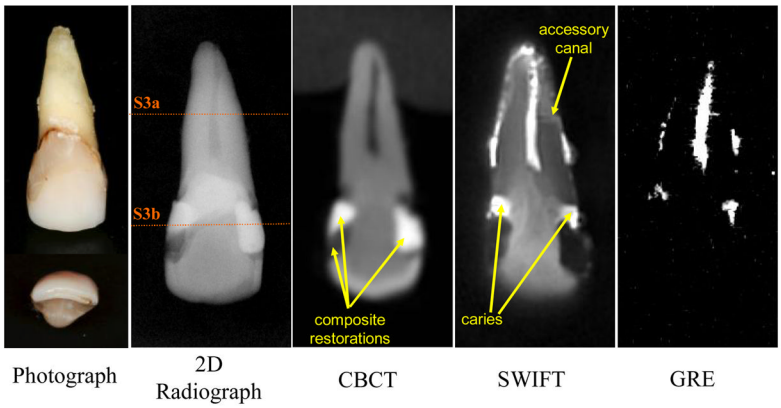

Figure 3.
A maxillary right central incisor (Tooth 2) with bilateral interproximal composite resin restorations and recurrent caries, imaged with different modalities. (SWIFT: selected slices with FOV diameter 40 mm and isotropic voxel size 156 μm; CBCT: isotropic voxel size 200 μm).

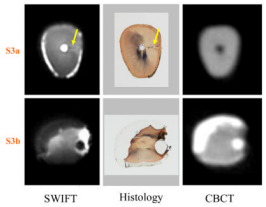

Figure 4.
Two cross-sectional slices of Tooth 2 (marked as S3a and S3b in Figure 3) are presented. The presence of an accessory canal (yellow arrows) is observed in the slice S3a within the SWIFT image and non-decalcified histology section, but not observed in the CBCT section. In slice S3b, the extent of the composite resin restorations are identifiable within the SWIFT section as well as in the CBCT and histological sections. The slice thickness is equal to 156 μm for SWIFT and 200 μm for CBCT images.

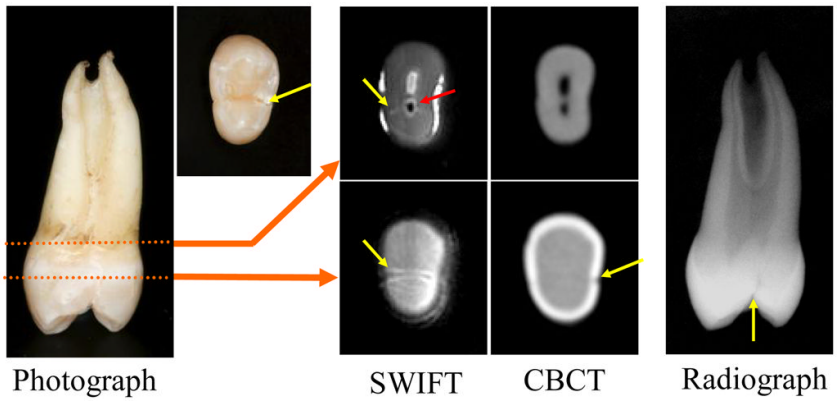

Figure 5.
A maxillary left first premolar with a complete lingual cusp fracture that has been reapproximated. In both radiographic image types and optical images the crack (yellow arrows) is hard to identify, but is easily observed in the SWIFT images. The red arrow delineates what is most likely air entrapped in the pulp canal when the crack was induced.

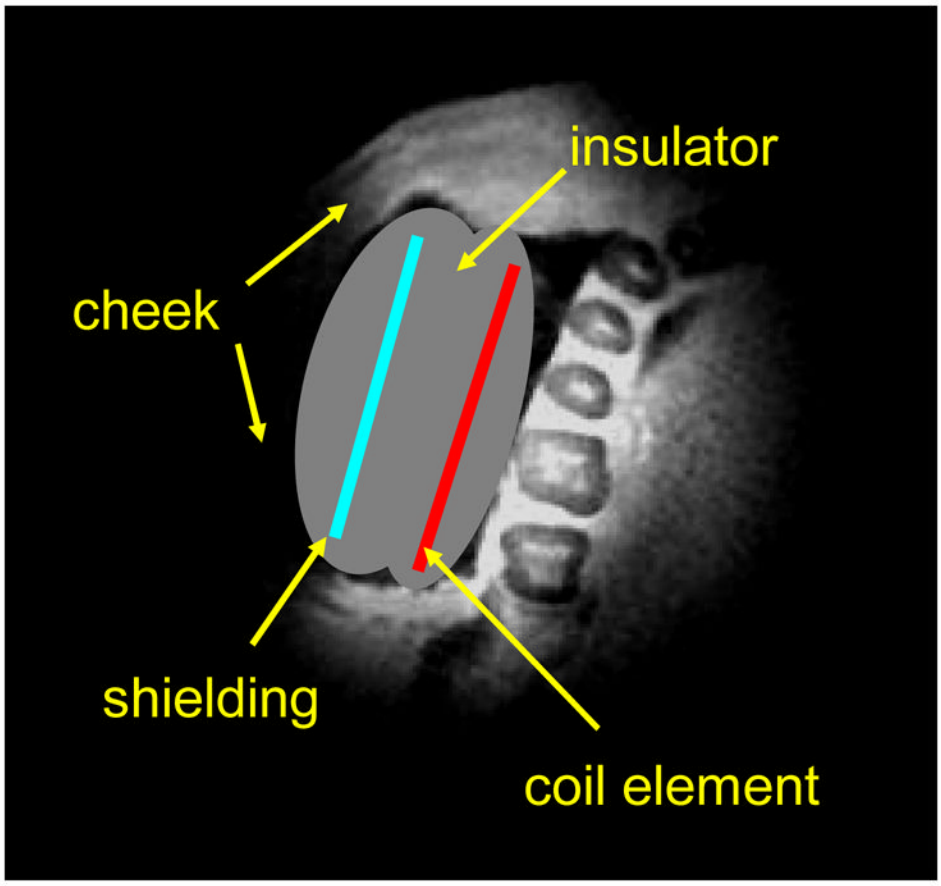

Figure 6.
Schematic illustration of the position of intra-oral RF coil for *in vivo* dental imaging experiments on the top of selected slice of a SWIFT image.

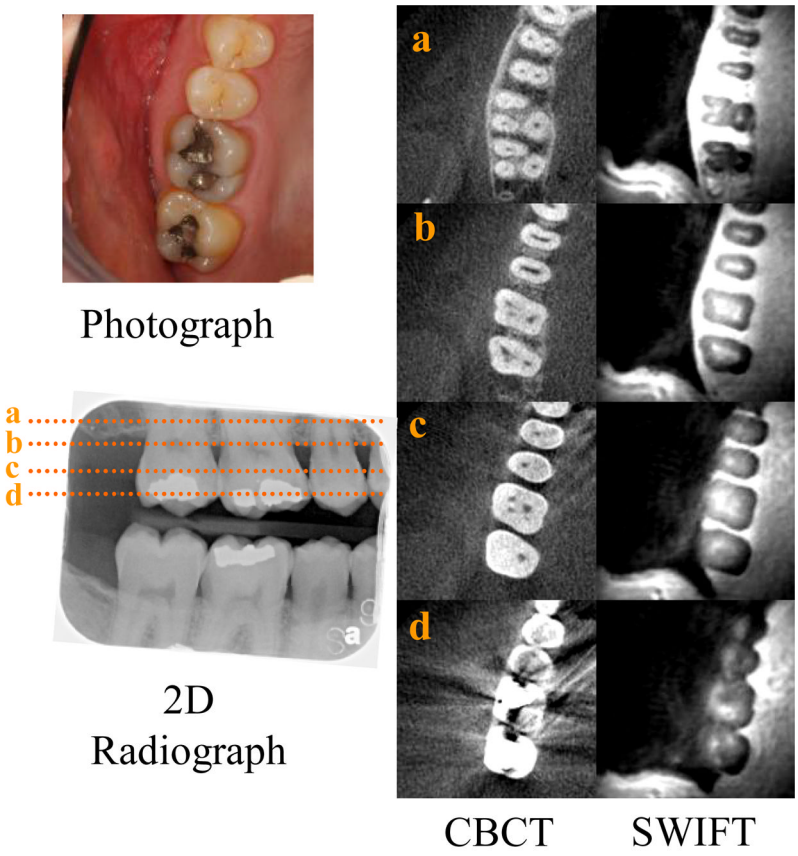

Figure 7.

In vivo images of the right posterior teeth. The photograph depicts the maxillary teeth that are also imaged with a traditional 2D radiograph used to detect interproximal caries. The dotted lines, represented by a, b, c and d, correlate with the cross-sectional CBCT and SWIFT images at those levels, from more superior closer to the root tip moving inferiorly to the crown of the teeth. Note the lack of image distortion associated with the occlusal amalgam restorations in the SWIFT sections compared to the CBCT sections. (SWIFT: selected slices with FOV diameter 110 mm and isotropic voxel size 430 μm).